Non-destructive evaluation of magnetic anisotropy associated with crystallographic texture of interstitial free steels

Mohsen Aghadavoudi Jolfaei [a],[*], Jun Liu [b], Lei Frank Zhou [a], Frenk Van Den Berg [c], Claire Davis [a]

[a] Warwick Manufacturing Group, University of Warwick, UK
[b] School of Engineering, Cardiff University, UK
[c] Tata Steel, IJmuiden, Netherlands

ARTICLE INFO

ABSTRACT

Interstitial free (IF) steels, as third generation of deep drawing steel, are used in the automotive industry for applications requiring good formability, strength and a superior surface quality. The formability is achieved by having a strong gamma fibre (γ-fibre) crystallographic texture and is quantified by measuring the r-value from tensile tests. Whereas the crystallographic texture is typically measured using EBSD or XRD on samples after careful surface preparation, it is desirable to be able to evaluate it non-destructively on production material. To do this aim, a magnetic anisotropy measurement is an attractive approach as the magnetic behaviour of steel is known to be affected by its crystallographic texture. A set of interstitial free steel samples, at different stages of recrystallisation process (i.e., commercially cold rolled and annealed to achieve fully and partially recrystallised microstructures) and consequently different texture components have been employed to study the measurement and possibility of model-wise predicting magnetic anisotropy in IF steels. In order to compare the predicted magnetic anisotropy to the measured values, a finite element (FE) microstructure model that takes into account crystallographic texture was applied.

The findings indicate that the non-destructive technique deployed in this study - a U-shaped electromagnetic (EM) sensor that can be placed onto a sheet specimen - is promising for a rapid assessment of the magnetic anisotropy in IF steels.

1. Introduction

Interstitial free steels (IF steels) find wide application in the automotive industry, due to their excellent formability. Crystallography texture is a key factor of interstitial free (IF) steel sheets as it is linked to plastic anisotropy, which is favourable to sheet metal formability [1]. Good formability is associated with high r-values (plastic strain ratio width to thickness) [1]. Steels that are suited for deep drawing applications should have an average r_m-value above 1.8 (normal anisotropy), while isotropic steels have an r_m-value of 1 [1]. Low planar anisotropy, Δr, and high normal anisotropy, r_m, are essential to ensure satisfactory drawability [2].

The main factors that influence the deep drawability of IF steel are the chemical composition, hot rolling parameters, subsequent cold rolling and annealing process [3,4]. The development of texture during various treatments including transformation of austenite to ferrite, hot rolling, cold deformation, and final continuous annealing (recrystallisation and grain growth) has therefore had significant amount of attention [3,5–7].

In terms of production, conventionally processed interstitial-free (IF) steel is hot rolled in the austenite region in a weakly textured hot band strip which is coiled in the ferritic state. Cold rolling causes the individual crystals to rotate by slip processes towards two significant sets of orientations, the α-fibre set, and the γ-fibre set [8].

The strength of these texture components, particularly the α-fibre, increases with cold rolling reduction [9,10] and during the final continuous annealing step, a texture with a strong γ-fibre develops [10] which is beneficial for excellent deep drawability [11,12]. It is desirable to be able to measure the intensity of texture that develops, for instance, considering magnetic anisotropy behaviour as this could be linked to the properties of final product and, if measured non-destructively, can be used for product quality control during production of steel.

It has been observed that the magnetic properties in ferromagnetic materials depend on the direction in which the properties are assessed if

there is strong crystallographic texture. Such magnetic anisotropy is due to the fact that there are certain orientations ($\langle 1\,0\,0 \rangle$ directions in steel) that are easier to magnetise (magnetic easy axis) [13,14] than the others.

Commercial electromagnetic (EM) sensor systems, including the HACOM, IMPOC, 3MA and EMspec^{TM} systems are employed to non-destructively monitor strip steels during steel production [15], with the former three used for final product characterisation (signals related to tensile strength) and the latter for phase transformation monitoring during cooling after hot strip rolling.

These systems do not currently measure (texture-related) magnetic anisotropy as they have not been designed for this purpose.

There are off-line electromagnetic (EM) systems used on products or laboratory samples measuring samples machined in different orientations/directions, such as Epstein Frame (EPF), Single Sheet Testers (SST) and Magnetic Barkhausen Noise (MBN) sensor. These techniques have been used extensively to characterise texture in electrical steels [16–19]. For example, Pluta et al. measured power loss in electrical steel taking into account the phenomenon of magnetic anisotropy showing that both hysteresis and additional eddy current loss components strongly depend on magnetic anisotropy [20].

Based on angular MBN measurements, Caldas-Morgan et al. proposed a method to assess magnetic anisotropy in ferritic stainless steel materials [21]. In this method the rotation speed should be low enough to minimize undesired effects such as eddy current damping and saturation of the amplifying circuit, however, the technique offers a practical experimental procedure used to find the macroscopic magnetic easy axis of ferromagnetic materials (qualitative evaluation of the anisotropy) [21]. Angular MBN has been applied to characterise magnetic anisotropy in pipeline steels [13,22,23]. However, Clapham et al. showed difficulties in finding a correlation between the angular dependence of the MBN energy and the crystallographic texture in API5L-X70 pipeline steel and their results suggested that plastic deformation and residual stress were responsible for the observed magnetic easy axis [22]. Magnetic anisotropy due to residual stresses has been considered by Buttle et al for measurements on rail steels [24,25]. Electromagnetic acoustic transducers (EMATs) have been used to assess texture in cold-rolled steel sheet and determine the r-value [26]. However, these approaches are restricted to near room temperature conditions and by the need for small stand-off distances. Laser-Ultrasonics has been used to determine elastic anisotropy and its coupling to crystallographic texture in stainless steel using galvano mirrors to direct the generating laser beam [27]. For IF steels, past laboratory research has been carried out to characterise recovery and recrystallisation of IF steel using magnetic properties, including dynamically at high temperature [12,28–30]. However, these studies have not considered anisotropy or whether texture can be assessed.

Since there is a business opportunity for a cost-effective and robust method to non-destructively evaluate crystallographic anisotropy in IF steels, the purpose of this work is the development of a method for measuring texture in strip steels samples using deployable EM sensor. This has been achieved by characterisation of the magnetic anisotropy of three IF steel sheets (partially / fully annealed cold rolled strip processed in a steel production plant as part of a plant trial) and microstructure-magnetic modelling considering the crystallographic texture. Measurements at different magnetic field strengths are reported along with a proposed EM sensor that can characterise local magnetic properties on strip samples.

2. Material and methods

Commercial IF steel strips with a thickness of 0.69 ± 0.01 mm as cold rolled and annealed to different recrystallisation levels were provided by Tata Steel Europe. Texture analysis was carried out using Electron Back Scattered Diffraction (EBSD) in a JEOL JSM-7800F0 scanning electron microscope with an accelerating voltage of 20 kV, a step size of 200 nm

and a specimen tilt of 70°. The grain size, Kernel Average Misorientation (KAM), Orientation Distribution Function (ODF), texture component and Inverse Pole Figure (IPF) were analysed using AZtec Crystal 2.1 software.

A laboratory based electromagnetic (EM) U-shaped sensor, operating at relatively low magnetic fields, has been developed to determine the magnetic anisotropy in the IF samples by measuring inductance (which is directly associated with the magnetic permeability of the steel sample) at angles varying from 0° to 90°, in steps of 15° with respect to the rolling direction (RD). Each test was examined with five repeat tests with zero lift-off (the distance between the sensor and the sample).

The EM sensor consists of two sensing coils with 50 turns of ϕ 0.16 mm insulated copper and one generation coil with 65turns of ϕ 0.20 mm insulated copper wire which were wound around the two legs of the U-shaped ferrite core with a bridge of 70 mm, leg diameter and leg lengths of 12 mm and 56 mm respectively. The EM sensor's sensing coil and exciting coils were driven by an Impedance Analyser Solartron (SL 1260A) with an AC excitation voltage of 3 V at frequencies from 10 Hz to 100 Hz. The excitation coil induces an alternating current magnetic field into the sample. The magnetic field produced by a multi-frequency EM sensor acts on a ferromagnetic target in two modes; first it tends to magnetise the sample, which increases the coil's inductance. Second, the alternating current magnetic field also induces eddy currents in the sample, which tend to oppose the driving current and reduce the coil's inductance. At a low frequency, the eddy currents in the sample are very weak; the contribution to the inductance change is mainly from the magnetisation of the sample and therefore the real inductance measured is related to the sample permeability. As the frequency is increased, the effect of the eddy currents becomes more dominant. Therefore, the real inductance versus frequency plot for the EM sensor has a plateau in inductance value at low frequency (below 100 Hz) in the region where the signal is independent of the electrical resistivity but dependent on the relative permeability of the sample. Therefore, the low field relative permeability value is determined from the experimental EM sensor measurement in that region.

In order to explore the links between real inductance measurements (as sensor signal) and relative permeability of the steel samples, a three-dimensional (3D) FE model using COMSOL Multi-physics was developed to simulate the U-shaped sensor with the AC/DC module. The COMSOL modelling approach is based on solving the Maxwell equations and boundary conditions. The geometry and details of the sensor/sample were set to be the same as the experimental set up.

Strip specimens of 300 mm × 30 mm were cut from selected IF steel sheets along 0°, 30°, 45°, 60° and 90° with respect to the RD respectively for permeability anisotropy measurements. A Brockhaus Single Sheet Tester (SST) was used to measure minor BH loops at a series of DC field amplitudes ranging from 50 A/m to 1000 A/m at frequencies of 50 Hz and 100 Hz.

A finite element microstructure model [31] that considers crystallographic texture using EBSD data has been used to predict the magnetic anisotropy in the IF steel samples. In this connection, a separate MAT-LAB code [32] was developed to generate polygons with continuous and smoothed grain boundaries from the EBSD data. The permeability values along the $\langle 1\,0\,0 \rangle$ and $\langle 1\,1\,1 \rangle$ direction used in the texture model have been estimated by fitting with the experimental measurements. Values of 2390 and 1720 have been assigned in the model as μ_{100} and μ_{111} respectively, considering magnetic field strength and a ratio of 1.39 between the μ_{100} and μ_{111} [33] and the previous work [31]. Full details for the model can be found in [31]. The modelling results have been experimentally validated using a laboratory based electromagnetic (EM) sensor.

3. Results and discussion

Three IF samples, including a partially recrystallised IF steel with high density of dislocations (IF-A), a partially recrystallised IF steel with

higher degree of recrystallisation and lower density of dislocations (IF-B) and a fully recrystallised IF steel (IF-C) were characterised and their EBSD micrographs are shown in Fig. 1. The grain boundary analysis map, Fig. 1(a)–(c), and the EBSD inverse pole figure (IPF) maps, Fig. 1(d)–(f) show a mixture of elongated areas and equiaxed recrystallised grains for both the partially recrystallised samples, IF-A and IF-B. However, the equiaxed grains in IF-A are extremely fine indicating it is in the early stage of recrystallisation. Fig. 1(a)–(c) also show the intergranular strain (misorientation 2–5°), low-angle grain boundaries (LAGBs, misorientation 5–15°), and high-angle grain boundaries (HAGBs, mis orientation >15°). The Kernel Average Misorientation (KAM) values from EBSD characterisation of the samples have been used to evaluate the recrystallisation fraction, based on the area fraction of the sample with KAM value below a critical value. In the present study, the KAM maps were calculated with a kernel size of 3×3 and a maximum threshold of 5°, Fig. 1(g)–(i). Due to the recrystallisation process, the HAGB fraction increases, the LAGB fraction decreases, and the KAM map of strain-free ferrite grains increases, Table 1.

The volume fractions of texture components are shown in Table 1 and Fig. 1 (k)-(m) where IF-A shows the highest percentage of α-fibre (55.3%) and the lowest percentage of γ-fibre (35.5%) and on the opposite side, IF-C displays the highest percentage of γ-fibre (69.2%) and the lowest percentage of α-fibre (16.7%). The ODF plots show that a mixed texture with a strong α-fibre and a weaker γ-fibre component in IF-A, a combination of a stronger γ-fibre and a weaker α-fibre component in IF-B and a well-developed γ-fibre for the fully annealed sample, IF-C, can be observed in Fig. 1(n)–(p).

Recrystallisation leads to the annihilation of dislocations by the nucleation and growth of defect free volumes, resulting in a new grain structure with a low dislocation density. The final recrystallisation texture is determined by the preferred nucleation of recrystallised grains of specific orientations [34].

Fig. 2 shows the subgrain distribution in the deformed α-fibre grains and γ- fibre grains in the partially recrystallised IF-A sample. Fine subgrains, due to recovery, are well developed in the γ-fibre grains but not in the α-fibre grains, which is likely to be due to the γ-fibre grains possessing a higher stored energy than the α-fibre grains from cold rolling [35]. These subgrains are the potential nuclei for recrystallisation. When one of these subgrains grows into a recrystallised grain, the orientation of the grain will be close to γ-fibre orientations.

Fig. 3 shows the measurements of the real inductance using the U-shaped EM sensor at a series of angles: 0°, 15°, 30°, 45°, 60°, 75° and 90° with respect to the RD for the three IF steel samples. It is worth mentioning that the EM sensor used in this study generates a low magnetic field (approximately 150–200 A/m) corresponding to reversible magnetisation processes in these steels [36].

A COMSOL model of the U-shaped sensor placed on a strip sample is shown in Fig. 4. It can be seen that the strong flux density (higher magnetic field strength) occurs between the sensor feet where the flux lines are mostly parallel to the length of the sensor.

Figure 5 shows predicted relative permeability values using 3D FE COMSOL modelling of the EM sensor for the IF samples from the angular dependence of real inductance measurements (Fig. 3) for the three IF steel samples.

It can be seen from Figs. 3 and 5 that the average inductance value and the relative permeability increase from IF-A to IF-C. A higher dislocation density in IF-A steel sample acts as pinning sites against magnetic domain wall movement, and results in lower inductance values (lower magnetic permeability). In the fully recrystallised sample IF-C, the low dislocation density reduces the pinning sites for magnetic domain wall movement, which, along with the larger grain size, means that the mean free path for domain wall movement increases, causing an increase in inductance/permeability.

In addition, grain size also plays a very significant role in the magnetic properties of steel. This is related to the formation of closure domains at the grain boundaries which deliver obstacles to domain wall motion during magnetisation. It is known that the permeability value is affected significantly by grain sizes in the range of 2.5–20 μm [37]. The grain size of IF-A sample (5.6 ± 0.4 μm) is smaller than IF-B (11.7 ± 1.3 μm) and IF-C (16.9 ± 1.6 μm). Therefore, the lowest value of inductance (permeability value) and the highest value among those samples are expected to be IF-A and IF-C respectively.

The three samples exhibit very different magnetic anisotropy as shown in the angular dependence of inductance and the predicted relative permeability illustrated in Figs. 3 and 5 respectively. In IF-A, Figs. 3(a), 5(a), the highest inductance value and the relative permeability are found for measurement along the rolling direction whilst in IF-B, Figs. 3(b), 5(b) are found in the range 60–90° (with respect to the rolling direction), although the anisotropy is very weak. In IF-C, Figs. 3(c) and 5(c), directions of 45° and 60° show higher induction/relative permeability values whilst the rolling direction shows the lowest value. The results from Figs. 3 and 5 also illustrate that the magnetic anisotropy behaviour varies with the stage of recrystallisation process in IF steel samples.

Fig. 6 shows the EBSD data, FE modelled microstructural geometry and predicted effective low magnetic field permeability map for the IF-B sample, following the approach described in [31] for modelling texture effects.

The predicted permeability anisotropy using the EBSD data for the three IF steel samples using the finite element microstructure model are presented in Fig. 7. It can be observed that the texture model predicts a strong anisotropic pattern for the fully recrystallised sample which agrees well with that of the measured real inductance and relative permeability value in Figs. 3(c) and 5(c) where the highest values of permeability (the texture model) and the EM sensor measurements (the inductance and/or the relative permeability) are seen for the 45° and 60° to the RD orientation and the lowest values are for the RD. There is good agreement for the IF-B sample where little anisotropy is observed for the inductance/relative permeability where the lowest values are seen for the 0° (RD) orientation and 30° whilst a similarly small anisotropy is predicted for the permeability texture model with the lowest value for the RD. The predicted permeability anisotropy using the texture model and measured permeability anisotropy using the EM sensor (the inductance and/or the relative permeability) also show reasonable agreement for the IF-A samples where the highest permeability and inductance/relative permeability values are seen for the 0° (RD) orientation and low values for the 90° (TD) orientation, although the texture model predicts lowest permeability values at 45° whereas the inductance/relative permeability values are lower than at 30° and 60° but not as low as the TD orientation. However, there is more scatter in values for this sample.

Regarding the quantitative ranges, it can also be seen that the texture model predicts a relatively small range for the three samples (range of 1500–2200), whilst the EM sensor outputs including the inductance and the relative permeability show a relatively larger range, 1.27–2.42 mH, and 1100–2150 respectively. This is because the texture model currently does not take into account the effect of the dislocation density present in unrecrystallised grains, which will affect the local magnetic properties (reducing the permeability values) – this will be more significant for the IF-A samples. In the partially recrystallised samples, where there is a mixture of α-fibre texture grains (typically unrecrystallised with a high dislocation density) and γ-fibre grains (typically recrystallised with a low dislocation density), the texture model predicted permeability will be higher than the measured permeability and the measured anisotropy will be affected predominantly by the recrystallised grains whereas the texture model predicts anisotropy from all grains. The consistency in all these permeability behaviours (real inductance) demonstrates that the present model is capable of capturing the crystallographic texture effects on magnetic anisotropy.

A grade of packaging steel (TH620) was used to determine how well the magnetic anisotropy measurement matches for different levels of texture in other strip steels. The EM sensor was employed to obtain the
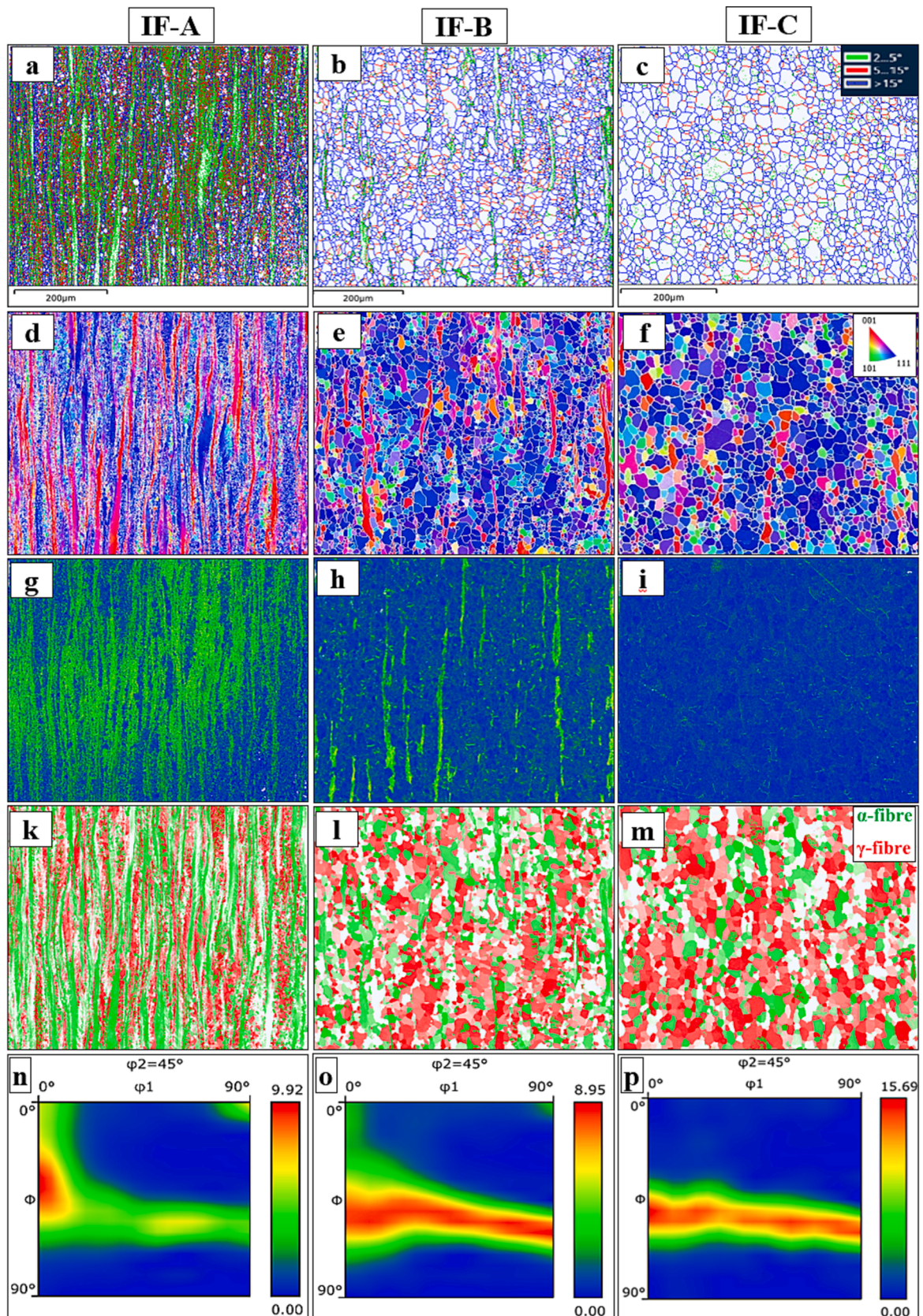
Fig. 1. Microstructural characterisation of IF-A, (left column), IF-B (middle column) and IF-C (right column): the grain boundary analysis map shows the grain misorientation in the IF steel samples, where green and red colour signify low-angle grain boundaries for misorientation (2–5°) and (5-15°) respectively, and high-angle grain boundaries (mis orientation > 15°) in blue colour (a, b, c), IPF maps for the ND pole (d, e, f), Kernel average misorientation map (KAM) (g, h, I), texture components where green colour represents α-fibre and red colour represents γ-fibre (k, l, m) and ODFs (φ2 = 45, half width 5°) (n, o, p). (For interpretation of the references to colour in this figure legend, the reader is referred to the web version of this article.)

Table 1

Low angle grain boundary (LAGB), and high angle grain boundary (HAGB) fractions (LAGB & HAGB), grain size and recrystallisation fraction in the three selected IF steel samples.

IF sample	LAGB fraction, %		HAGB fraction, % (Misorientation > 15°)	Grain size* (µm)	Recrystallisation %	Texture component	
	(Misorientation, 2–5°)	(Misorientation, 5–15°)				α-fibre ⟨110⟩// RD	γ-fibre ⟨111⟩// ND
IF-A	36.2	31.2	32.6	5.6 ± 0.4	43	55.3%	35.5%
IF-B	18.1	15.6	66.3	11.7 ± 1.3	88	27.2%	58.8%
IF-C	13.5	12.8	73.7	16.9 ± 1.6	100	16.7%	69.2%

*The elongated areas were excluded.
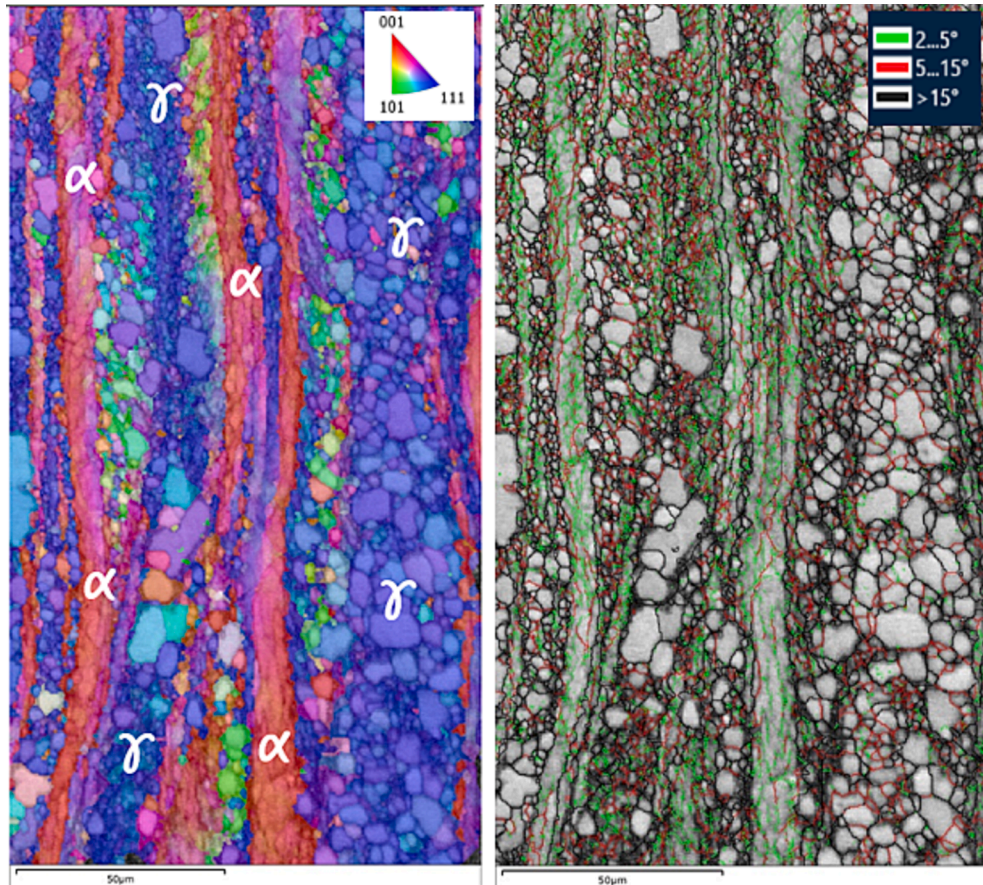
Fig. 2. Subgrain development according to the grain orientation in fine grained IF-A sample, extremely fine equiaxed grains indicating it is in the early stage of recrystallisation (a) image quality map overlaid by inverse pole figure (IPF) map, α-fibre and γ- fibre grains are indicated (b) band contrast micrograph with low and high-angle grain boundaries.

angular dependence of inductance at a series of angles from 0°, 15°, 30°, 45°, 60°, 75° and 90° with respect to the RD. Fig. 8(a) shows an IPF map from the microstructure and a combination of α-fibre and γ-fibre can be revealed from the ODF map in Fig. 8(b).

There is a good agreement between the texture model (the model parameters are identified as $\mu_{100} = 479$ and $\mu_{111} = 345$, which reflect the lower applied field used compared to the original model set up in [26] and the experimental results of the EM sensor for this sample. The angular dependence of inductance/permeability and magnetic anisotropy behaviour when compared with the partially and fully recrystallised IF samples, indicates a weaker texture for this microstructure; the ODF map, Fig. 8, shows that the maximum intensity is 5.18, compared to 15.89 for the recrystallised IF steel (IF-C) and 8.95 for the partially recrystallised IF steel (IF-B) where only weak anisotropy was seen.

A study was carried out to see the effect of magnetic field strength on the permeability anisotropy behaviour to determine if the current EM sensor design/operation parameters could to be altered to provide

greater sensitivity to anisotropy, in a similar manner applied when characterising DP steels (for phase fraction and grain size) and reported in [38]. Strip samples of 300 mm × 30 mm were cut from fully recrystallised IF steel sheet, IF-C, along 0°, 30°, 45°, 60° and 90° with respect to RD respectively, and the Brockhaus single sheet tester (SST), was used to measure minor loop permeability at a series of DC field amplitudes ranging from 50 (A/m) to 1000 (A/m) frequencies of 50 Hz and 100 Hz.

Fig. 9 shows the measured incremental permeability values as a function of the measurement directions at different minor loop amplitudes. It can be seen that the permeability anisotropy behaviour is, in general, highly sensitive to the minor loop amplitude.

At low amplitude 50 (A/m), Fig. 9(a), an almost isotropic permeability behaviour is observed, the permeability increases with the magnetic field amplitude until reaching a maximum incremental permeability values of 2750 and 2060 for the frequencies of 50 Hz and 100 Hz respectively for the 60° orientation with respect to the RD at a field strength of 300 (A/m) where the strongest anisotropic behaviour
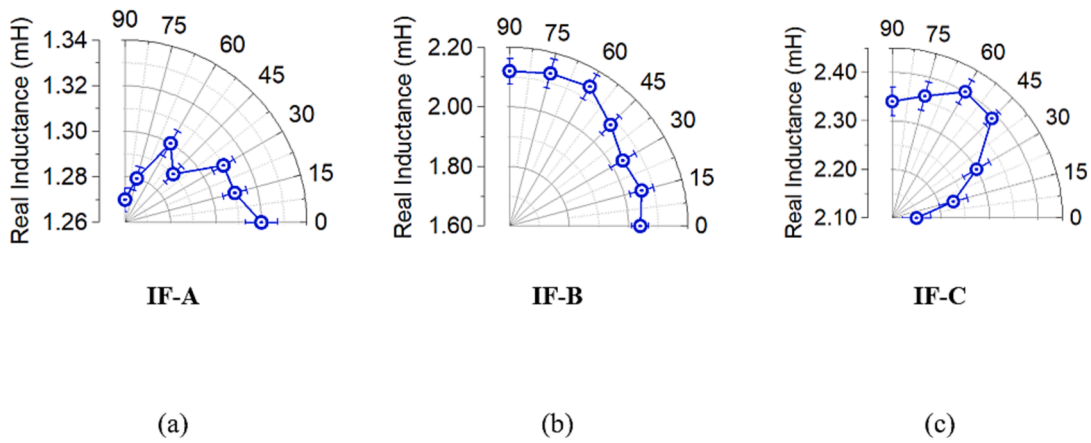
Fig. 3. Angular dependence of real inductance measurements for IF-A, IF-B and IF-C using the EM sensor.
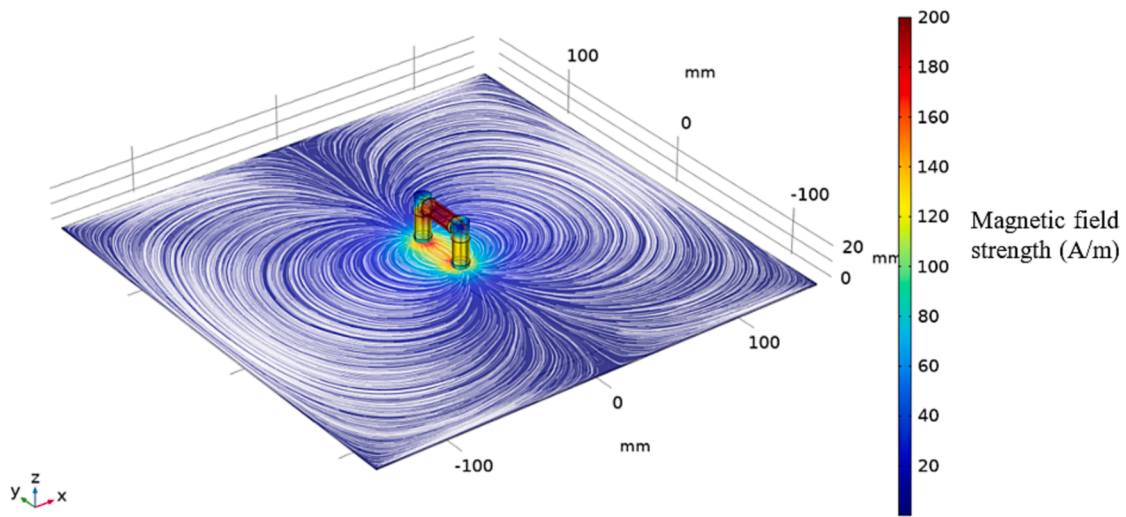

Fig. 4. FE modelling of the U-shaped EM sensor to estimate the low field permeability of specimens.
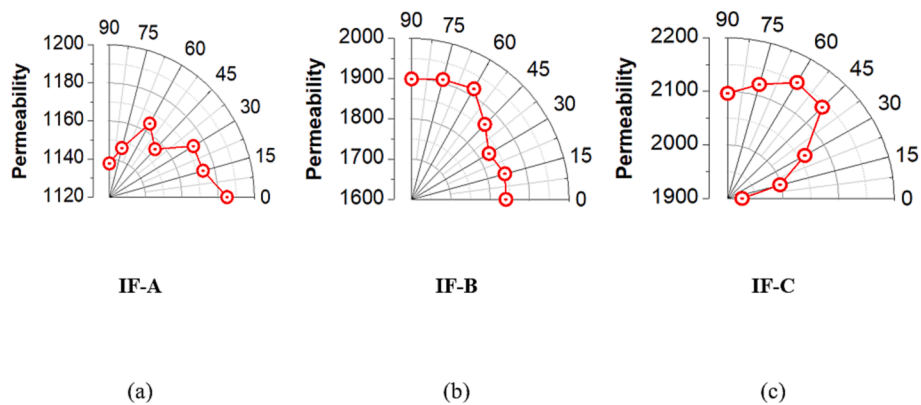

Fig. 5. Predicted relative permeability values from COMSOL modeling derived from the angular dependence of real inductance measurements for IF-A, IF-B and IF-C.

can be found, Fig. 9(e), and then drops followed to a more isotropic permeability behaviour at higher amplitudes Fig. 9(f)(g). It can be seen that due to the eddy current effect, the permeability values at a frequency of 10 Hz are higher than the permeability values at frequency of 100 Hz.

Fig. 10 shows a series of minor loops with the different magnetic field amplitudes ranging from 50 (A/m) to 1000 (A/m) in the fully

recrystallised IF sample, IF-C, for the specimen at 90° with respect to RD. The shape of the minor loops alters depending on the amplitude; at low amplitudes, they have lenticular shapes, while at greater amplitudes, they take on sigmoid shapes.

The incremental permeability is physically regarded as the gradient of the loop, which has a highest value for the minor loop at a magnetic field of 300 (A/m). At higher magnetic field, the sample starts to reach
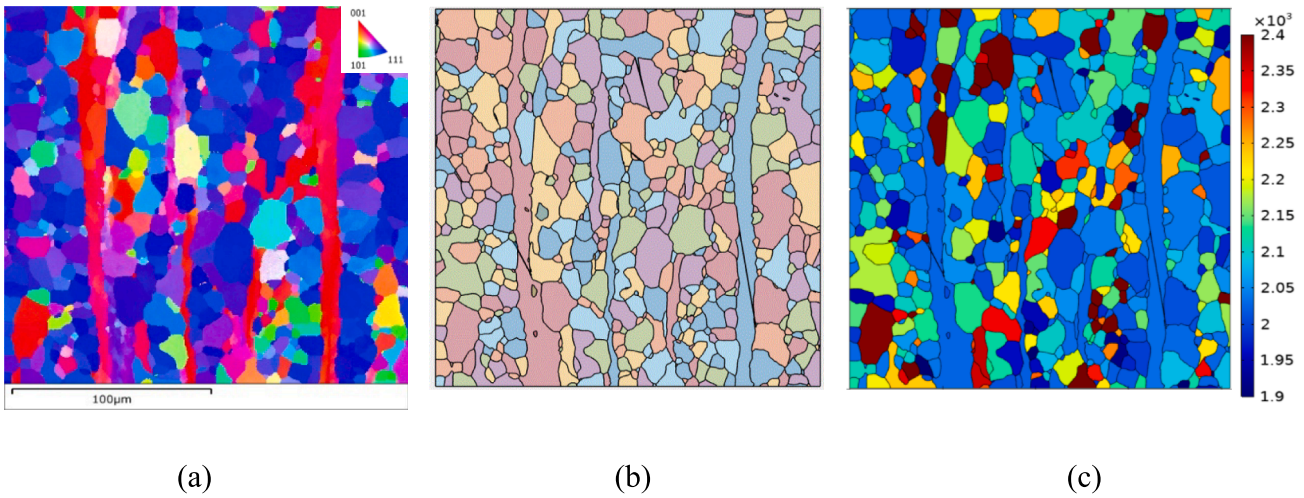
Fig. 6. The finite element microstructure model (a) imported inverse pole figure (IPF) maps, (b) converted the EBSD data into the model (ready for the FE geometry), (c) predicted low magnetic field permeability map for IF-B sample.
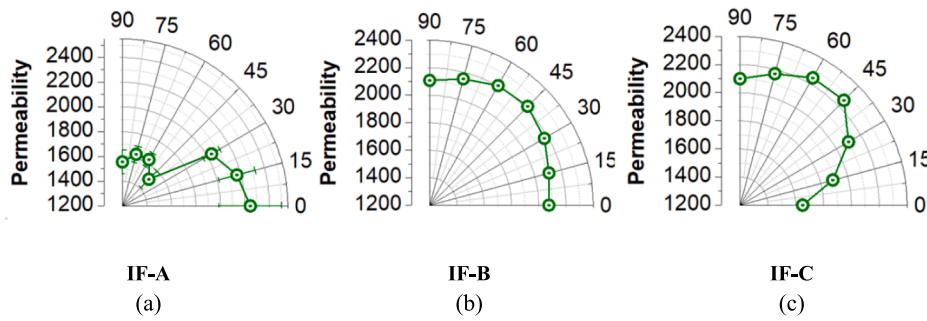

Fig. 7. Predicted magnetic anisotropy using the texture model for IF-A, IF-B and IF-C samples.
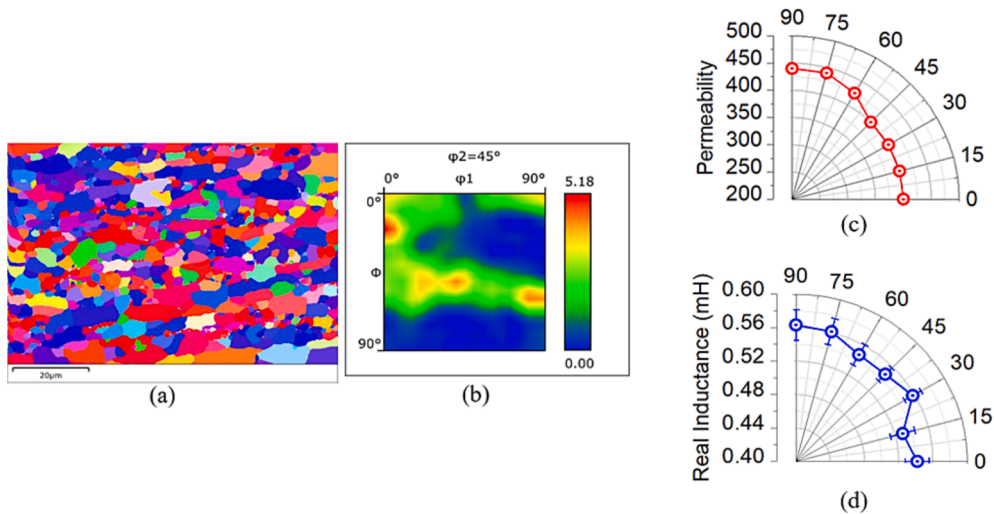

Fig. 8. Inverse pole figure (IPF) map (a), ODF map (b) predicted magnetic permeability using the texture model (c) and the angular dependence of inductance at a series of angles from 0°, 15°, 30°, 45°, 60°, 75° and 90° with respect to the RD (d) in the packaging steel sample.

saturation point where the shape of minor loop changes into a sigmoid shape and magnetic anisotropy decreases showing isotropic behaviour.

The permeability value depends on the magnetic field strength [38]; if it is assumed that a similar amount of magnetic field strength was applied to the sample (taken as 200 A/m based on the COMSOL model for the sensor), the EM sensor predicted permeability values ranged from

1940 to 2150 for sample IF-C (11% difference between minimum and maximum values) and the SST measurement showed a range of 2030 to 2570 (27% difference between minimum and maximum values). This discrepancy between the predicted permeability from the U-shaped sensor and the measured permeability value using SST technique can be linked to how the EM sensor operates/works as it can be seen from Fig. 4
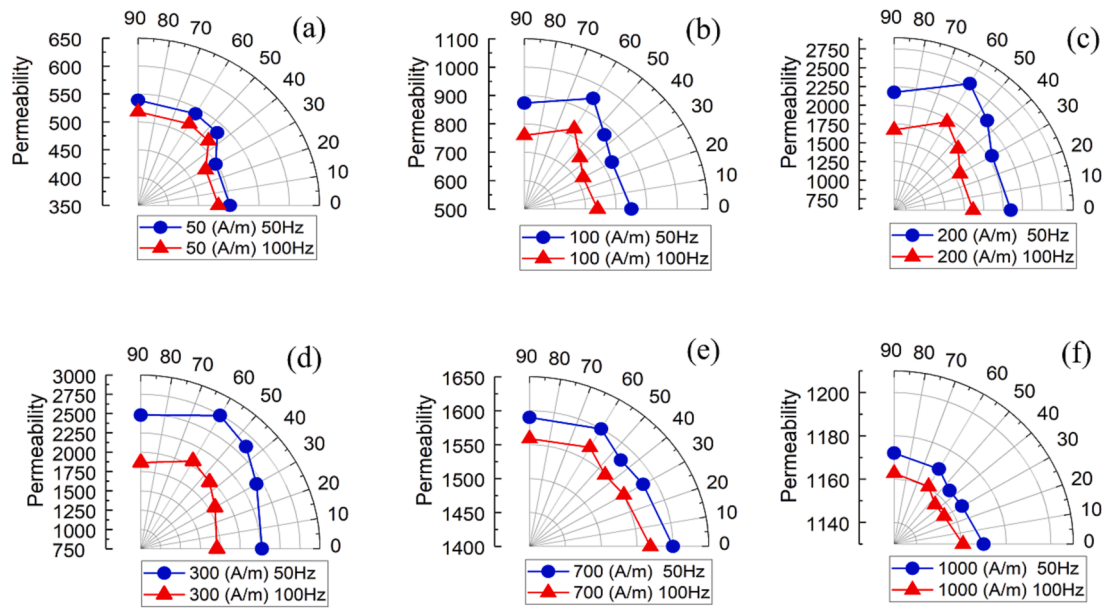
Fig. 9. Incremental magnetic permeability as a function of the measurement directions at different minor loop amplitudes in the fully recrystallised IF sample.
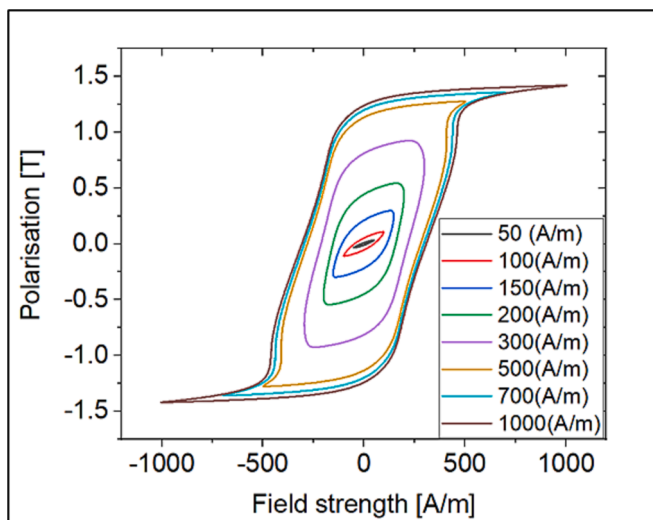

Fig. 10. A series of minor loops in the fully recrystallised IF- C sample along 90° with respect to RD.

that most of the flux is concentrated between the feet and parallel to the length of the sensor, therefore the sensor predominantly measures the magnetic permeability along that axis. Although there will be some flux at different orientations therefore the sensor will not be as sensitive to texture as e.g. the SST measurements where all the flux in the sample is parallel to the measurement direction.

The results show that the EM sensor measurement (inductance value, related to the low field relative permeability) is able to differentiate the state of the recrystallisation process in IF steel, as has been reported previously [28], since the dislocation density is significantly reduced during the recrystallisation process, and the nucleation of new strain free grains leads to an effective grain refinement followed by some grain growth. Consequently, as a result of the change in the dislocation density and the grain size, the average real inductance value increases. In addition, the angular inductance measurement reveals the formation of new grains after recrystallisation inevitably alters the crystallographic texture and the texture factors giving different values (direction dependence) that can be quantified. It is worth noting that selecting an

appropriate magnetic field amplitude (where the effect of anisotropy is more significant) is important for detecting permeability anisotropy behaviour. In this connection based on the previous work [38] a field strength close to where maximum permeability occurs but less than the coercivity point is recommended.

4. Conclusions

The study of ferromagnetic anisotropy has received the attention of numerous investigators and various methods for its experimental detection have been devised. For the present work an easy to deploy rapid method for characterising magnetic anisotropy, using an electromagnetic (EM) sensor, has been developed which can be used with sheet steels. In this study, steels with different texture components have been used to investigate the measurement and prediction of magnetic anisotropy, using an FE based model, in IF steels. The angular inductance measurement from the EM sensor was able to reveal the anisotropy from the local magnetic response as well as the change of the overall magnetic properties with respect to the change of the material status during recrystallisation. The proposed approach can be successfully applied for experimental evaluation of the magnetic anisotropy in IF steels. A finite element microstructure model that considers crystallographic texture has been used to predict the magnetic anisotropy in the IF steel samples based on the measured texture. The model potentially can be used in a reverse manner to characterise texture from magnetic measurements. The present model is anticipated to be used to provide the permeability anisotropy for predicting sensor measurements for low field EM sensors used for monitoring steel quality during processing and/or for the interpreting the EM sensor signals to infer the texture of the steel. In addition, the permeability maps serve as an enhanced visual and quantitative indication of the textures as a supplement to inverse pole figure (IPF) maps.

The angular dependence of inductance showed that for an IF steel in the partially recrystalised (the cold rolled condition), the highest inductance value is seen along rolling direction due to the strong α fibre texture, whilst the highest value for the fully recrystallised sample is found at 45°−60° (with respect to the rolling direction) related to the strong γ fibre texture.

It was observed that the anisotropy intensity behaviour in fully recrystallised IF steel increases with the applied magnetic field amplitude until reaching a maximum anisotropy value at a certain applied

field amplitude which then decreases at higher applied magnetic field amplitude. Selection of an appropriate applied magnetic field for the steel being investigated is recommended to maximise the anisotropy measurement, in this work the deployable EM sensor generates a maximum field strength of around 200 A/m in the sample, less than the coercivity value, and this was sufficient to reveal the magnetic anisotropy.

CRediT authorship contribution statement

Mohsen Aghadavoudi Jolfaei: Conceptualization, Data curation, Formal analysis, Investigation, Methodology, Validation, Visualization, Writing – original draft, Writing – review & editing. **Jun Liu:** Software, Validation. **Lei Frank Zhou:** Methodology. **Frenk Van Den Berg:** Writing – review & editing, Project administration, Resources. **Claire Davis:** Supervision, Funding acquisition, Project administration, Writing – review & editing.

Declaration of Competing Interest

The authors declare that they have no known competing financial interests or personal relationships that could have appeared to influence the work reported in this paper.

Data availability

The authors do not have permission to share data.

Acknowledgements

References

[1] S. Hoile, Processing and properties of mild interstitial free steels, Mater. Sci. Technol. 16 (2000) 1079–1093.

[2] L.-L. Hao, L. Li, C.-Y. Qiu, J.-G. Wang, X. Zhou, Y.-L. Kang, Texture development and properties of Ti-IF steels produced by different hot-rolling processes, J. Iron Steel Res. Int. 26 (2019) 310–320.

[3] R. Zheng, R. Song, W. Fan, Effects of annealing cooling rates on mechanical properties, microstructure and texture in continuous annealed IF steel, J. Alloy. Compd. 692 (2017) 503–514.

[4] H. Kawabe, S. Matsuoka, T. Shimizu, O. Furukimi, K. Sakata, Y. Ito, Effect of increase in r-value on press formability for cold-rolled steel sheet, JSAE Rev. 23 (2002) 139–141.

[5] T. KM, C. Jung, P. Wray, G. CI, D. AJ, Evolution of texture in ferritically hot rolled Ti and Ti+ Nb alloyed ULC steels during cold rolling and annealing, ISIJ Int. 44 (2004) 404–413.

[6] K.M. Lee, M.Y. Huh, O. Engler, Quantitative analysis of micro-textures during recrystallization in an interstitial-free steel, Steel Res. Int. 83 (2012) 919–926.

[7] G. Bhargava, L. Patra, S. Pai, D. Mishra, A study on microstructure, texture and precipitation evolution at different stages of steel processing in interstitial free high strength steels, Trans. Indian Inst. Met. 70 (2017) 631–637.

[8] P. Juntunen, P. Karjalainen, D. Raabe, G. Bolle, T. Kopio, Optimizing continuous annealing of interstitial-free steels for improving deep drawability, Metall. Mater. Trans. A 32 (2001) 1989–1995.

[9] D. Verma, S.K. Shekhawat, N. Mukhopadhyay, G. Sastry, R. Manna, Development of texture in interstitial-free steel processed by equal-channel angular pressing, J. Mater. Eng. Perform. 25 (2016) 820–830.

[10] S. Dutta, V. Rajinikanth, A.K. Panda, A. Mitra, S. Chatterjee, R.K. Roy, Effect of annealing treatment on mechanical and magnetic softening behaviors of cold rolled interstitial-free steel, J. Mater. Eng. Perform. 28 (2019) 2228–2236.

[11] D.V. Edmonds, Designing with microalloyed and interstitial-free steels, Handbook of Mech. Alloy _ Des. (2004) 321.

[12] A. Martinez-de-Guerenu, K. Gurruchaga, F. Arizti, Nondestructive characterization of recovery and recrystallization in cold rolled low carbon steel by magnetic hysteresis loops, J. Magn. Magn. Mater. 316 (2007) e842–e845.

[13] P. Martínez-Ortiz, J.A. Perez-Benitez, J.H. Espina-Hernandez, F. Caleyo, J. Hallen, On the estimation of the magnetic easy axis in pipeline steels using magnetic Barkhausen noise, J. Magn. Magn. Mater. 374 (2015) 67–74.

[14] A. Aharoni, Introduction to the Theory of Ferromagnetism, vol. 109, Clarendon Press, 2000.

[15] J. Shen, L. Zhou, W. Jacobs, P. Hunt, C. Davis, Real-time in-line steel microstructure control through magnetic properties using an EM sensor, J. Magn. Magn. Mater. 490 (2019), 165504.

[16] T. Yonamine, F.J. Landgraf, Correlation between magnetic properties and crystallographic texture of silicon steel, J. Magn. Magn. Mater. 272 (2004) E565–E566.

[17] N. Leuning, S. Steentjes, M. Heller, S. Korte-Kerzel, K. Hameyer, On the correlation of crystallographic macro-texture and magnetic magnetization anisotropy in non-oriented electrical steel, J. Magn. Magn. Mater. 490 (2019), 165485.

[18] L. Kestens, S. Jacobs, Texture control during the manufacturing of nonoriented electrical steels, Text. Stress Microstruct. (2008).

[19] F. Landgraf, T. Yonamine, M. Emura, M. Cunha, Modelling the angular dependence of magnetic properties of a fully processed non-oriented electrical steel, J. Magn. Magn. Mater. 254 (2003) 328–330.

[20] W. Pluta, Calculating power loss in electrical steel taking into account magnetic anisotropy, Prz. Elektrotech 1 (2018) 102–105.

[21] M. Caldas-Morgan, L. Padovese, Fast detection of the magnetic easy axis on steel sheet using the continuous rotational Barkhausen method, NDT and E Int. 45 (2012) 148–155.

[22] L. Clapham, C. Jagadish, D. Atherton, The influence of pearlite on Barkhausen noise generation in plain carbon steels, Acta Metall. Mater. 39 (1991) 1555–1562.

[23] P. Martínez-Ortiz, J.A. Perez-Benitez, J.H. Espina-Hernandez, F. Caleyo, N. Mehboob, R. Grössinger, J. Hallen, Influence of the maximum applied magnetic field on the angular dependence of Magnetic Barkhausen Noise in API5L steels, J. Magn. Magn. Mater. 401 (2016) 108–115.

[24] D. Buttle, V. Moorthy, B. Shaw, J. Lord, Determination of residual stresses by magnetic methods, 2006.

[25] S. Santa-Aho, A. Sorsa, A. Nurmikolu, M. Vippola, Review of railway track applications of Barkhausen noise and other magnetic testing methods, Insight-Non-Destruct. Test. Cond. Monit. 56 (2014) 657–663.

[26] R. Murayama, K. Fujisawa, H. Fukuoka, M. Hirao, Development of an on-line evaluation system of formability in cold-rolled steel sheets using electromagnetic acoustic transducers (EMATs), NDT and E Int. 29 (1996) 141–146.

[27] M. Malmström, A. Jansson, B. Hutchinson, Application of laser-ultrasonics for evaluating textures and anisotropy, Appl. Sci. 12 (2022) 10547.

[28] L. Zhou, F. Wu, R. Hall, C. Davis, Electromagnetic sensors for in-situ dynamic microstructure monitoring of recovery and recrystallisation in interstitial free steels, J. Magn. Magn. Mater. 551 (2022), 169187.

[29] E. Schmidová, M. Neslušan, J. Ondruš, K. Trojan, M. Pitoňák, F. Klejch, S. K. Ramesha, Monitoring of plastic straining degree of components made of interstitial free steel after uniaxial tensile test by the use of barkhausen noise technique, Steel Res. Int. (2021) 2100597.

[30] K. Gurruchaga, A. Martinez-de-Guerenu, M. Soto, F. Arizti, Efficacy of magnetic inductive parameters for annealing characterization of cold rolled low carbon steel, IEEE Trans. Magn. 44 (2008) 3839–3842.

[31] J. Liu, C. Davis, Tensorial permeability microstructure model considering crystallographic texture and grain size for evaluation of magnetic anisotropy in polycrystalline steels, Philos. Mag. 101 (2021) 1224–1244.

[32] J. Liu, EBSD Polygonizer, 2020.

[33] R.M. Bozorth, Ferromagnetism, 1993.

[34] E.F. Ferdinand Knipschildt, Nucleation of recrystallization, Mater. Sci. Technol. (2022) 1–15.

[35] M. Yasuda, K. Murakami, K. Ushioda, Recrystallization Behavior and Formation of {411}< 148> Grain from α-fiber Grains in Heavily Cold-rolled Fe-3% Si Alloy, ISIJ Int. 60 (2020) 2558–2568.

[36] M.A. Jolfaei, Characterisation of Advanced High Strength Strip Steels Using Electromagnetic Sensor System, University of Warwick, University of Warwick, 2019.

[37] L. Zhou, C. Davis, P. Kok, Steel microstructure–magnetic permeability modelling: the effect of ferrite grain size and phase fraction, J. Magn. Magn. Mater. 519 (2021), 167439.

[38] M. Aghadavoudi Jolfaei, L. Zhou, C. Davis, Consideration of magnetic measurements for characterisation of ferrite–martensite commercial Dual-Phase (DP) steel and basis for optimisation of the operating magnetic field for open loop deployable sensors, Metals 11 (2021) 490.